Cell Stem Cell
Article

Mouse Germ Line Stem Cells Undergo Rapid and Stochastic Turnover

Allon M. Klein,[1,2] Toshinori Nakagawa,[3] Rie Ichikawa,[4] Shosei Yoshida,[3,4,5,*] and Benjamin D. Simons[2,6,*]
[1]Department of Systems Biology, Harvard Medical School, 200 Longwood Avenue, Boston, MA 02115, USA
[2]Cavendish Laboratory, Department of Physics, J.J. Thomson Avenue, University of Cambridge, Cambridge CB3 0HE, UK
[3]Department of Pathology and Tumor Biology, Graduate School of Medicine, Kyoto University, Kyoto, 606-8501, Japan
[4]Division of Germ Cell Biology, National Institute for Basic Biology, National Institutes of Natural Sciences, Okazaki, 444-8787, Japan
[5]Department of Basic Biology, School of Life Science, Graduate University for Advanced Studies (Sokendai), Okazaki, 444-8787, Japan
[6]MRC Cancer Cell Unit, Hutchison-MRC Research Centre, Cambridge CB2 0XZ, UK
*Correspondence: shosei@nibb.ac.jp (S.Y.), bds10@cam.ac.uk (B.D.S.)
DOI 10.1016/j.stem.2010.05.017

SUMMARY

In cycling tissues, adult stem cells may be lost and subsequently replaced to ensure homeostasis. To examine the frequency of stem cell replacement, we analyzed the population dynamics of labeled stem cells in steady-state mouse spermatogenesis. Our results show that spermatogenic stem cells are continuously replaced, on average within 2 weeks. The analysis exposes a simple and robust scaling behavior of clone size distributions that shows stem cell replacement to be stochastic, meaning that stem cells are equipotent and equally likely to be lost or to multiply to replace their neighbors, irrespective of their clonal history. The surprisingly fast rate of stem cell replacement is supported experimentally by 3D clone morphology and by live-imaging of spermatogonial migration. These results suggest that short-lived stem cells may be a common feature of mammalian stem cell systems and reveal a natural mechanism for matching the rates of cell proliferation and loss in tissue.

INTRODUCTION

In adults, cycling tissues are supported by stem cells, which persist throughout life, maintaining their own population while giving rise to differentiating progeny. How stem cell function is maintained to ensure tissue homeostasis is an important open question that remains to be elucidated in most tissues and in mammals in particular. Indeed, mammalian stem cell research has been largely dependent on posttransplantation reconstitution and postinsult regeneration assays that do not necessarily reflect the steady state. However, investigation of undisturbed tissue is essential for understanding stem cell regulation in steady state, which may differ from that seen under conditions of stress (e.g., Nakagawa et al., 2007; Simon and Frisén, 2007).

Spermatogenesis provides one of the most well-characterized stem cell systems in mammals. In the mouse testis, spermatogenesis occurs in the seminiferous tubules, where germ cells at various stages of differentiation reside in multiple layers (Figures 1A–1C). Spermatogonia are functionally heterogeneous mitotic cells, including self-renewing stem cells and transit-amplifying cells that proceed to terminal differentiation. The basal (i.e., the most peripheral) layer of seminiferous tubules hosts all stages of spermatogonia; subsequently, spermatocytes (meiotic cells) relocate toward the lumen as they transform into round, and then elongated, spermatids (haploids) (Figure 1D). This process of differentiation occurs periodically in accordance with the seminiferous epithelial cycle of 8.6 days: the germ cells move through four layers until the matured sperm are released into the lumen 35 days later. All the germ cells reside between Sertoli cells, the somatic cells that line the inner part of the seminiferous tubules (de Rooij and Russell, 2000; Russell et al., 1990).

Stem cell function resides in a small spermatogonial subpopulation, consisting of A_s (A_{single}; singly isolated cells), A_{pr} (A_{paired}; cysts of interconnected cell pairs), and A_{al} ($A_{aligned}$; interconnected cells in sycytial cysts of 4, 8, 16, and occasionally 32 cells). However, unequivocal identification of the stem cells within this subpopulation has not been achieved. It has been recently shown that, in addition to their varying cyst length, the A_s, A_{pr}, and A_{al} spermatogonia are also characterized by variable levels of gene expression (Figure 1E): *GFRα1* and *nanos2* are expressed in a large subset of A_s and A_{pr} that is capable of steady-state self-renewal, while many of A_{al} are $Ngn3^+$ and tend to differentiate. However, $Ngn3^+$ cells are also capable of switching to a $GFR\alpha1^+$ state and contributing to the stem cell pool, both in steady-state spermatogenesis as well as in regenerating tissue postinjury (Nakagawa et al., 2007, 2010; Sada et al., 2009; Suzuki et al., 2009; Barroca et al., 2009).

While it remains difficult to unequivocally identify stem cells at a cellular level, lineage-tracing studies can characterize the "macroscopic" dynamics of long-lived, stem cell-derived clones in steady-state spermatogenesis, from which one can infer the underlying stem cell behavior (Nakagawa et al., 2007). In a recent study, using a tamoxifen-inducible *cre* recombinase-LoxP system, we showed that single stem cell-derived clones form cohesive patches along seminiferous tubules, indicating that stem cells and their differentiating progeny occupy adjacent areas. In addition, over the course of the reproduction period, some stem cells lose their function (they might differentiate without self-renewing or die) and are replaced by newly

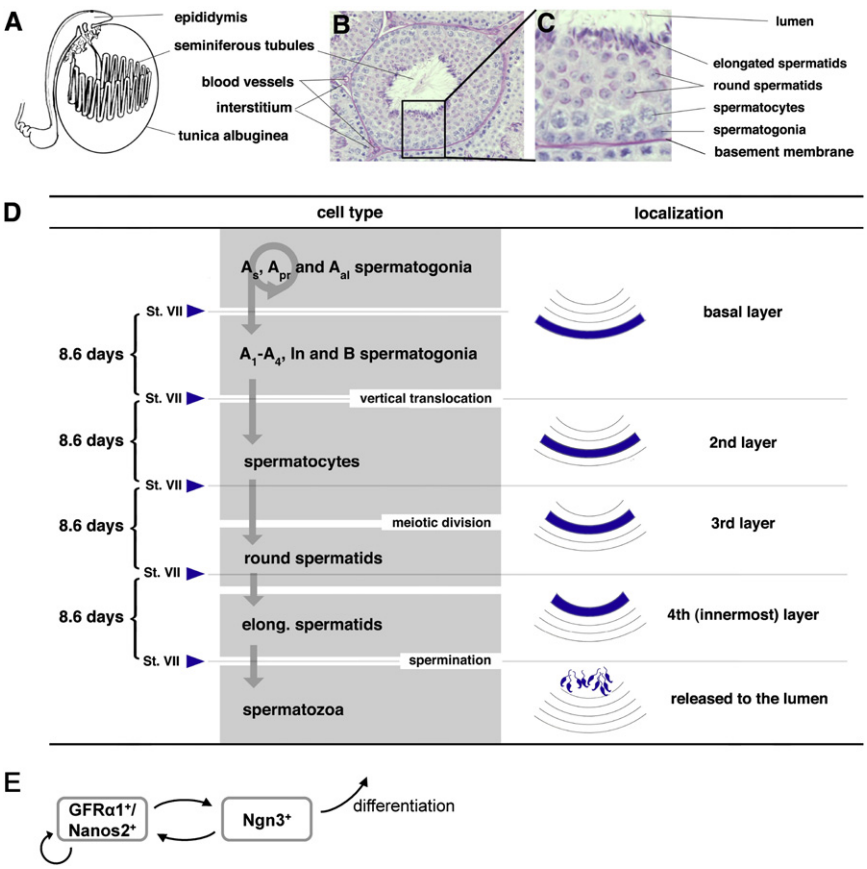

Figure 1. Organization of Spermatogenesis in Mouse Testes

(A) In mouse testis, convoluted seminiferous tubules form loops connected to the rete testes, the outlet of sperm, and are packed within the tunica albluginea (capsule).

(B and C) PAS-hematoxylin-stained cross-sections show the four layers of differentiating germ cells, from the basement membrane to the lumen.

(D) Steps of spermatogenic differentiation and stratification. The basal layer hosts A_s, A_{pr}, and A_{al} spermatogonia, in which the stem cell function resides, as well as their differentiating progeny A_1, A_2, A_3, A_4, In, and B spermatogonia. At stage VII of the seminiferous epithelial cycle (lasting 8.6 days), the latter enter into meiosis, becoming spermatocytes, followed by vertical translocation to the second layer. The periodic nature of these events is reflected in the synchronous migration through the third and fourth stratified cell layers, as shown in (C), before release into the lumen.

(E) Relation of gene expression to self-renewal potential in A_s, A_{pr}, and A_{al} spermatogonia. *GFRα1* and *nanos2* are expressed in spermatogonia capable of steady-state self-renewal, while those expressing Ngn3 tend to differentiate but are also capable of switching to *GFRα1* expression and self-renewing (Nakagawa et al., 2010).

generated stem cells that are derived from neighboring stem cells. This finding indicated that, even after its establishment, the stem cell population is not static but instead undergoes continuous turnover that keeps the total stem cell number constant (Nakagawa et al., 2007). However, the process that underlies stem cell replacement, its frequency, and its significance to steady-state spermatogenesis remained unknown.

In this study, we have investigated the ongoing replacement of the spermatogenic stem cells in steady state through a quantitative analysis of pulse-labeling results, including data from Nakagawa et al. (2007). Specifically, we have made use of a powerful form of data analysis borrowed from statistical physics, which exposes systemic patterns of stem cell replacement known as ''scaling'' features of the clone-fate data. This analysis is capable of revealing whether clones expand as a result of an inequality between stem cells or replacement of aging stem cells or whether the stem cells are equipotent and act stochastically. The analysis also exposes the frequency at which stem cells are lost. Given the novelty of the scaling analysis in germ line stem cell biology, we accompany the analysis with computational modeling to provide a simple picture of stem cell turnover in spermatogenesis. Through this, one may gain insight into how replacement actually occurs between sparsely distributed stem cells all along the seminiferous tubules. Finally, we provide evidence in support of our findings through pulse-labeling and live-imaging of spermatogonia in undisturbed testes.

RESULTS

Clonal Analysis Reveals a "Scaling" Behavior of Labeled Clones

To characterize stem cell behavior in steady-state spermatogenesis, we first performed a detailed mathematical analysis of the clone size data obtained in previous pulse-labeling experiments (Nakagawa et al., 2007). In this study, the fate of $Ngn3^+$ spermatogonia was analyzed by inducing the hereditary expression of LacZ following a tamoxifen pulse (Figure 2A). In steady-state spermatogenesis, although the majority of the labeled $Ngn3^+$ cells differentiate and exit the tissue, a fraction of cells retain (or perhaps recover) stem cell potential, generating patches that may persist over many months. Such behavior is consistent with the expression of GFRα1 (and probably also Nanos2) in the $Ngn3^+$ cell-derived clones as recently reported in Nakagawa et al. (2010). Indeed, pulse-labeling of $Nanos2^+$ spermatogonia (Sada et al., 2009) provides clone-fate dynamics consistent with that seen in *ngn3*-based labeling experiments (Figure S1 available online). Upon labeling, persistent LacZ-positive cells were found clustered in patches along the seminiferous tubules (Figure 2B). Continuity of LacZ-tagged cells in these patches, and their scarcity, indicates that each labeled patch is derived from a single $Ngn3^+$ cell labeled at induction. In our experiments, the number and length of the resulting labeled patches were tracked up to 14 months postlabeling (Figures 2C and 2D).

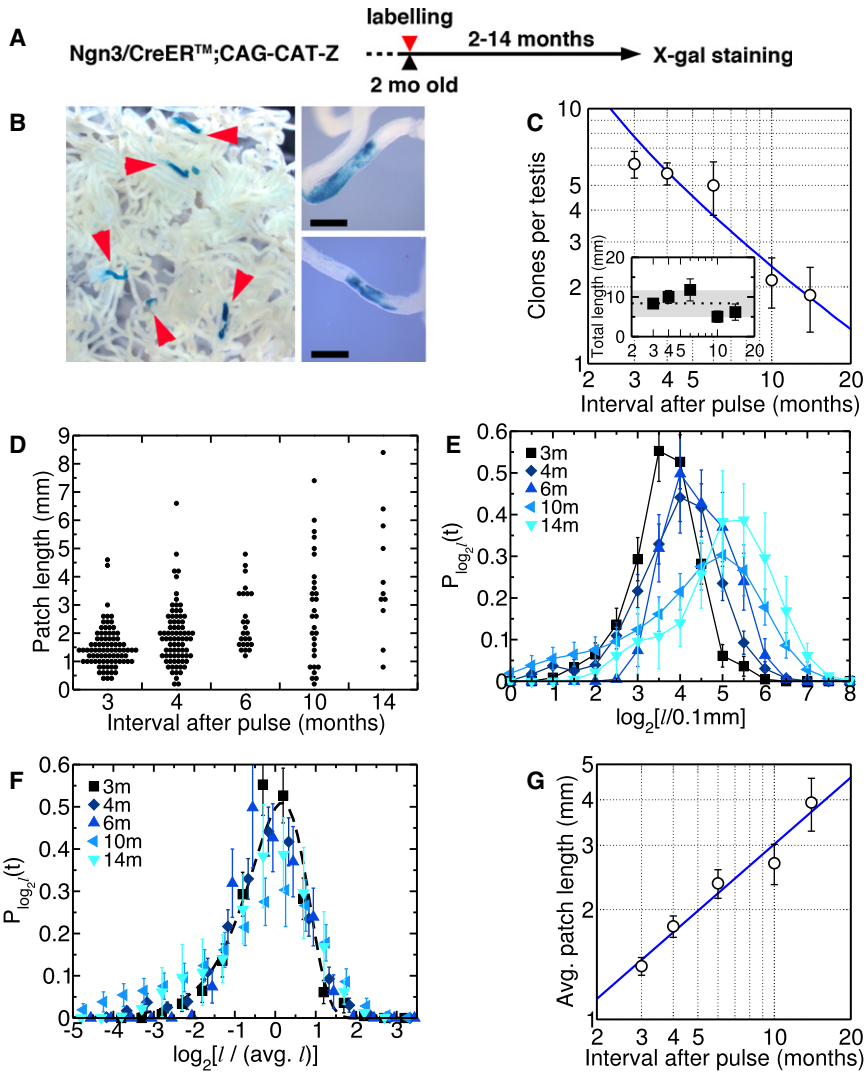

Figure 2. Clonal Fate Analysis Reveals Scaling Behavior in Steady-State Spermatogenesis

(A) Experimental schedule in genetic labeling experiments (Nakagawa et al., 2007).

(B) Appearance of X-gal-stained patches in the seminiferous tubules 3 months after induction. Scale bars, 0.2 mm.

(C) Log-log plot of the number of persistent labeled patches over time in steady state (error bars show SEM; see also Figure S1). The curve shows a fit of the neutral drift model (see later in Figure 3). Inset: The average total length of labeled patches per testis over time postlabeling (error bars show SEM). The values fluctuate about the time-averaged mean (dotted), consistent with the labeled cells turning over in a manner representative of the total cell population. The gray region shows the predicted standard deviation due to statistical fluctuations arising from the small number of patches per testis.

(D) Raw patch-length data, showing the length of all individual patches scored at progressive time points. Data at 3 and 10 months is reproduced from Nakagawa et al. (2007).

(E and F) To investigate the scaling properties of the patch-length data shown in (D), the length distributions are plotted in (E) as a function of the logarithm of the segment length, $\log_2[l/0.1\ \mathrm{mm}]$ (error bars show SEM). By replotting the same distributions against the segment length rescaled by the average length, $\log_2[l/\langle l(t)\rangle]$, in (F), one sees that all the clone-fate data sits on a single universal curve (shown dashed) described by Equation 1 and conforming to the theory in Equation 2. The data points in (F) correspond to those in (E).

(G) Log-log plot of the average patch length over time (error bars show SEM). The straight line fit indicates that the data follows a power law of the form $\langle l(t)\rangle = (Dt)^{\alpha}$, where D is the scaling constant and α is a dimensionless scaling exponent. Least-squares fitting reveals that $\alpha = 0.55 \pm 0.06$, and $D = 0.89 \pm 0.16\ \mathrm{mm}^2/\mathrm{month}$ (mean ± SEM).

From 3 months postlabeling, the patch number was found to decrease while persistent patches expand continually (Figures 2C and 2D). Yet, as the total patch length (i.e., the sum of all patch lengths per testis) remains constant throughout the chase period (Figure 2C, inset), we are able to deduce that the cells that maintain the labeled patches are representative of the entire stem cell population. Solely from this observation, we conclude that mouse spermatogenesis does not simply depend on the self-renewal of "orthodox" long-lived stem cells that divide only asymmetrically into a stem and a short-lived transit-amplifying (TA) cell. If this were the case, then the number and size of labeled patches would be constant, reflecting the fraction of stem cells labeled at induction. Instead, steady-state spermatogenesis involves an ongoing loss of clones that is compensated by expansion of neighboring clones through stem cell multiplication (Nakagawa et al., 2007).

We therefore asked whether the extinction and expansion of the stem cell clones follow a pattern. To this aim, we analyzed the dynamics of the labeled patch-length *distribution*, which reflects the underlying stem cell behavior. In particular, we were inspired by a recent study of cell lineage in mouse interfollicular epidermis (IFE), where the fate choices of epidermal progenitor cells were inferred from a striking "scaling behavior" of the clone size distributions (Clayton et al., 2007). Here, "scaling" implies that the clone size distributions maintain their form and merely dilate (or "scale") over time, an empirical behavior that admits very few models of progenitor cell fate. The appearance of scaling indicates that a simple process governs the behavior of the entire system, regardless of the complex interactions between multiple components that the system may involve. In addition to its identification in clonal analysis in IFE, scaling behavior is found in a wide range of biological phenomena, including metabolomics, biomechanics, bacterial motility, and pattern formation during development (Brown et al., 2000; Spence, 2009).

Remarkably, we find that the patch-length data in mouse spermatogenesis also show a clear scaling behavior. To see this, we define $P_l(t)\Delta l$ as the probability of finding a labeled clone with

a segment length lying in the range l to $l+\Delta l$ at a time t postinduction; analysis shows that this probability distribution conforms to a simple scaling behavior (see Figures 2E and F),

$$P_l(t) = \frac{1}{\langle l(t)\rangle} f(l/\langle l(t)\rangle), \quad (1)$$

where $f(x)$ denotes the (as yet unspecified) "scaling function," and the entire time dependence of the distribution is contained in the average patch length, $\langle l(t)\rangle$. Formally, referring to Figure 2F, the patch-length distributions from the family of time points "collapse" onto a single curve when plotted against the length "rescaled" (i.e., divided) by the average length, $l/\langle l(t)\rangle$. This collapse is similar (but as we will see, distinct) to that observed in mouse IFE (Clayton et al., 2007).

In addition to the collapse of the patch-length distributions, the steady-state stem cell dynamics exhibits additional features commonly observed in scaling systems in biology and physics. First, the average patch length shows a good fit to a power law $\langle l(t)\rangle = (Dt)^{\alpha}$, where D is a "scaling constant" and α is a dimensionless exponent. This is apparent from the linear relation in a log-log plot of the average patch length over time (Figure 2G), $\log(\langle l(t)\rangle) = \alpha\log(t) + \alpha\log(D)$. The value of α can vary between different scaling systems, and it is related to the particular rules governing each system. In our case, a least-squares fit gives a slope $\alpha = 0.55 \pm 0.06$ and a scaling constant $D = 0.89 \pm 0.17\text{mm}^{1/\alpha}$/month (mean ± sem). The slope α is close to 0.5, indicating that the average patch length grows approximately as the square root of time. We shall soon show that this pattern of square-root growth has far-reaching implications for the behavior of germ line stem cells.

Stem cell regulation and maintenance involve complex interactions between cells and their environment. However, the observed scaling behavior suggests that clonal extinction and expansion can be characterized by just a single (as yet unspecified) process. Any system involving multiple significant processes would give rise to a dynamics dependent on multiple parameters and not just the single scaling parameter, D, as actually observed (Supplemental Experimental Procedures). In the following, by addressing several models of stem cell behavior, we will show that the range of clone-fate data is consistent with only one.

Clone-Fate Dynamics Rule Out a Heterogeneous Stem Cell Pool of Long- and Short-Lived Subpopulations, as Well as Extensive Stem Cell Migration

To characterize the process of stem cell replacement, we looked for population models that exhibit the scaling behavior seen in the patch-length data. We first considered the possibility that the labeled patches derive from a mixture of "long-lived," asymmetrically dividing stem cells and "short-lived" stem cells that produce a smaller number of progeny, where the former gives rise to the latter. This model would explain both the decay in patch number and the increase in average patch size (Figure 2C and 2G), resulting from the gradual loss of short-lived stem cell-derived patches. However, there are two observations that rule against this model. First, in this case, the number of labeled patches should eventually stabilize once all short-lived stem cells have exited the tissue; however, in reality, the patch number declines inexorably throughout the entire 14 months of experiment, which covers most of the reproduction period of mice. Significantly, clones derived from Nanos2^{+} cells (Sada et al., 2009) follow the same quantitative pattern of ongoing decay over several months (Figures S1A and S1B). Second, as short-lived stem cells exit the tissue, the smallest patches should disappear and the persisting patches should become less heterogeneous; instead, the observed patch-length distribution becomes more heterogeneous over time (Figure 2D), with small patches persisting throughout the entire experiment. While the existence of a long-lived asymmetrically dividing stem cell population cannot be strictly ruled out, if it exists, its role in steady-state spermatogenesis must be sufficiently small as to have no noticeable effect on the clone-fate data.

Two further models of clonal expansion are ruled out based on the clone-fate data: one is that the entire labeled patch population might consist of stem cells that expand to replace unlabeled shorter-lived progenitor cells in the surrounding area. Such a pattern of expansion predicts a linear growth of the average patch length and not square root as observed, a patch number per testis that becomes constant, and a failure of the observed scaling (Supplemental Experimental Procedures). Finally, we may rule out the possibility that patches might expand through the migration and subsequent intermingling of long-lived stem cells. If this were the case, labeled and unlabeled stem cells would mix, leading to extensive fragmentation (or dilution) of large patches. By contrast, patches are seen to remain cohesive with high-labeling density over the entire 14 months of experiment.

Stem Cell-Derived Clones Evolve through Neutral Drift

Based on the preceding results, we conclude the following:

(1) Labeled patches are *not* supported by a mixture of long-lived and short-lived stem cell populations.
(2) The labeled patches do *not* have a growth advantage over the surrounding cells.
(3) Germ line stem cells do *not* migrate significantly past their neighbors.

These constraints point at a particular class of population dynamics, known as *neutral drift* models. These models deal with a population of equipotent components that multiply or are lost in a stochastic (i.e., neutral) manner. These models have been intensely studied since their introduction over a century ago in mathematical finance (Bachelier, 1900); their best known example in biology is the neutral theory of molecular evolution (Kimura, 1983). In the case of spermatogenic stem cell replacement, the neutral drift hypothesis is that all the stem cells are equipotent and can neutrally replace their neighbors. In other words, over long enough times, each stem cell is considered equally likely to self-renew or be lost irrespective of its clonal history. As described in the following sections, this hypothesis fits all of the observed patch-length data and provides quantitative predictions for the stem cell replacement rate.

To understand the neutral drift dynamics in mouse seminiferous tubules, let us temporarily consider stem cell replacement only along the length of the tubule (Figure 3A); we will shortly address the full picture, including replacement around the tubule

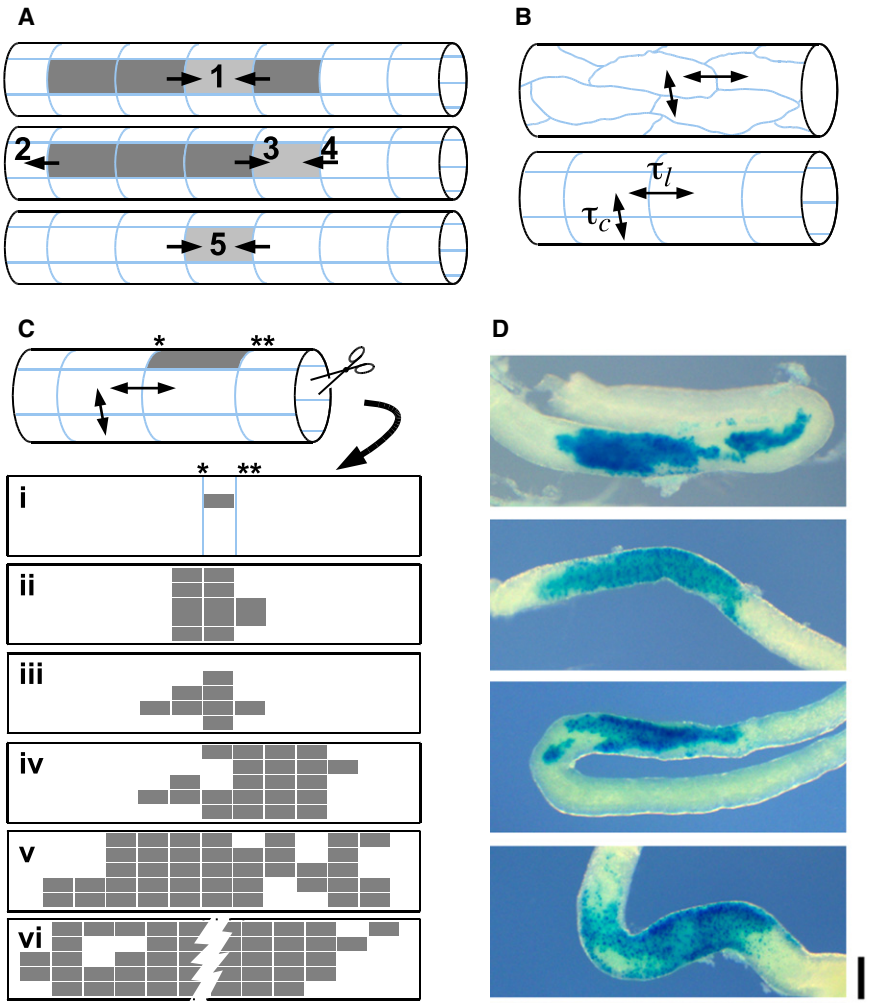

Figure 3. Models of Stochastic Stem Cell Replacement and Neutral Drift

(A) A simplified "one-dimensional" model of patch evolution along the length of the seminiferous tubule, involving several contiguous labeled stem cells and their differentiating progeny (gray units). The schematic shows the possible outcomes of stem cell loss in the center of a labeled clone (case 1), at its boundary (cases 2–4), and of the final labeled stem cell in a clone (case 5), leading to clone extinction. Regions in which the stem cells are lost (through differentiation) are shown faded. The resulting clonal expansion and contraction leads to neutral drift of the clone boundary (see main text).

(B) A more realistic (two-dimensional) model of patch evolution. The effect of stem cell replacement (top) is captured by a simple model (bottom) involving a regular arrangement of stem cells that stochastically replace their neighbors with an average replacement time τ_l along the tubule length and τ_c around its circumference.

(C) Snapshots from a typical simulation of the model (with $\tau_l = \tau_c$). To visualize the entire cylindrical cross-section, the tubule has been "cut" and flattened out as shown. The simulation starts with one labeled stem cell supporting a small region of the tubule (gray) at $t = 0$ (panel i); progressive panels show the patch size at times $t/\tau_l = 5$, 10, 25, 50, and 100 (full simulation results in Figure S2).

(D) A closer view of the patch morphology 3 months after the pulse. Note their irregular boundary with a striking similarity to the simulations in (C). Bar, 200 μm.

circumference. In this thought experiment, if a labeled cell population in the middle of a labeled clone becomes extinct because of stem cell loss, it will be replenished by the progeny of stem cells that inhabit either of the neighboring regions (Figure 3A, case 1). In this case, since cells in both neighboring regions belong to the labeled clone, the continuity of labeling is maintained. By contrast, if the extinction takes place in an unlabeled region neighboring the labeled region, its repopulation by a labeled stem cell will lead to an expansion of the labeled clone (Figure 3A, case 2). Similarly, if a labeled stem cell is lost on the clone periphery, repopulation by neighbors may lead to its restoration, leaving the patch length unchanged (Figure 3A, case 3), or to a reduction in its length through expansion of an unlabeled clone (Figure 3A, case 4). The clone disappears if the last stem cell is lost (Figure 3A, case 5).

Significantly, this dynamic exhibits the very same characteristics seen in our experiment. The clone size distributions conform to a scaling behavior (shown explicitly in the following section), while the average patch length exhibits a square root relationship with time (Figure 2G). Therefore, this simple model already captures the essential features of the observed patch-length data.

The proposed behavior assumes the coordinated replacement of stem cells by nearby, or adjacent, stem cells (Figure 3A). We also considered an alternative hypothesis (also a type of neutral drift), in which the multiplication and loss of stem cells is determined cell-autonomously, i.e., independently of adjacent stem cell fate. However, such cell-autonomous behavior, which is seen for example in mouse IFE, predicts a linear clonal growth and corresponds to a different scaling behavior from that observed in the data (Supplemental Experimental Procedures and Clayton et al., 2007). We can therefore conclude that the loss and replacement of stem cells is indeed coordinated between neighboring stem cells in spermatogenesis.

To complete our description of the neutral drift theory, a more realistic model should accommodate neutral drift around the cylindrical boundary of the seminiferous tubules as well as along their length (i.e., in two dimensions). The patch dynamics here are essentially the same as that seen in the aforementioned 1D model and in the actual patches (Supplemental Experimental Procedures and Figures S2A–S2C). To illustrate the 2D model behavior, we conducted simulations of the patch dynamics using a simplified representation of the tubules (Figure 3B). In this model, the regions supported by individual stem cells are approximated to identical rectangular segments that are aligned regularly in a lattice pattern with K stem cells surrounding the circumference. It is assumed that replacement

occurs only between adjacent stem cells, with average replacement rates of $1/\tau_l$ along the tubule *l*ength and $1/\tau_c$ around the tubule *c*ircumference (Figure 3B); (this idealized arrangement assumes exactly four nearest neighbors per stem cell). Figure 3C represents snapshots of a typical simulation of the 2D model, starting with one labeled stem cell, followed by equipotent stem cell replacement both along and around the tubules. Despite the simplicity of this model, the in silico-generated patches closely resemble the in vivo patches: large simulated patches remain contiguous and show a similar irregular shape, including some minor fragmentation at the patch edges, with less than 3% of simulated clones undergoing any further fragmentation (Figure 3D and Supplemental Experimental Procedures).

Germ Line Stem Cells Are Frequently Replaced during Steady-State Spermatogenesis

To quantitatively test the neutral drift hypothesis, we then exploited the mathematical properties of the dynamics. For that purpose, it was necessary to define the typical length of the region supported by a single stem cell along the seminiferous tubule to be l_0. In addition, we defined the transit time, T_T, as the typical time required for the complete turnover of the differentiating population by stem cells. T_T must be longer than the time required for A_1 spermatogonia to differentiate into matured spermatozoa and be released, i.e., 5 weeks (Russell et al., 1990; see Figure 1D). On the other hand, most of the patches derived from labeled transit-amplifying cells exit within 7 weeks postlabeling (Figure S1A). Therefore, T_T is constrained to lie in the range of 5–7 weeks.

With these definitions, at times in excess of the replacement time, τ_l, one may show that the labeled patch-length distribution acquires the scaling form

$$P_l(t) = \frac{\pi l}{2\langle l(t)\rangle^2} \exp\left[-\frac{\pi l^2}{4\langle l(t)\rangle^2}\right], \quad (2)$$

where $\langle l(t)\rangle$ is the average labeled patch length of persisting clones at time t (Supplemental Experimental Procedures). At early times the average patch length grows linearly with a growth rate $R = l_0/\tau_l$, whereas at times much longer than T_T, the average patch length grows as the square root of time, $\langle l(t)\rangle = (Dt)^{1/2}$, with a scaling constant $D = \pi {l_0}^2/\tau_l$. Such behavior matches closely to the observed average patch-length data (Figure 2G). Moreover, comparing Equations (1) and (2), one may see that the theory also recovers the scaling behavior of the patch-length distribution, with a scaling function $f(x) = (\pi/2)\, x \exp[-\pi x^2/4]$ that involves no adjustable parameters. Significantly, the rescaled patch-length distribution predicted from $f(x)$ (dashed line in Figure 2F) provides an excellent fit to the observed distributions, providing strong support for the neutral drift dynamics. Moreover, using the estimate T_T = 6 weeks, a log-log plot of the survival curve confirms that the patch number, too, behaves as predicted by theory (Figure 2C).

From the formulae for the scaling constant $D = \pi {l_0}^2/\tau_l$ and the initial growth rate $R = l_0/\tau_l$, the average stem cell replacement time can be expressed as $\tau_l = D/\pi R^2$. The patch growth rate during the earliest measurable period (5 weeks to 8 weeks postlabeling) was found to be $R^* = 0.81 \pm 0.09$ mm/month. This figure should be less than the initial growth rate since the growth rate is slowing down, i.e., $R > R^*$. Combined with the value of $D = 0.89 \pm 0.17$ mm^2/month measured earlier, this implies that the replacement rate is remarkably short, with $\tau_l < 1.9 \pm 0.5$ weeks.

From the two formulae above, we can also infer that the average length of the region associated with each stem cell is $l_0 = D/\pi R < 0.35 \pm 0.08$ mm. In addition, an important implication of neutral drift dynamics is that, at any time point after labeling, some surviving patches will include just a *single* stem cell and its progeny, although their abundance decreases with time. Indeed, from 5 weeks to 14 months, the very smallest patch at each time point was roughly constant in their length of 0.37 ± 0.14 mm (mean ± SEM). The appearance of a constant length for the smallest patches, and its similarity to the predicted value of l_0, again supports the validity of the neutral drift model.

Individual Germ Line Stem Cells Support a Small Region of the Seminiferous Tubules

Although the theoretical analysis is based on 'macroscopic' measurements of stem cell-derived patches over long periods, it predicts characteristics of individual stem cell behavior. First, differentiating cells derived from a single stem cell are expected to occupy a small region of the seminiferous tubule with an average length of 0.35 ± 0.08 mm or less. This figure contradicts a recent length estimate of 1.38mm, which was based on the assumption that individual stem cells are long-lived (Nakagawa et al., 2007). Second, neighboring stem cells stochastically replace each other with a rate of more than once per two weeks. In the following sections, we evaluated the validity of these predictions from detailed analyses of spermatogonial behavior.

First, we re-evaluated the size of the region supported by a single stem cell based on the neutral drift model. For this purpose, we analyzed the size of patches observed as early as five weeks after pulse-labeling (Figure 4A). Within this chase period, a labeled self-renewing stem cell is expected to reveal the spatial organization of a single stem cell-derived lineage by reconstituting the entire hierarchy of differentiating cells. Because five weeks should allow for multiple stem cell replacement events on average ($\tau_l < 1.9 \pm 0.5$ weeks), some of the observed patches at this point are expected to consist of multiple stem cells and their progeny, while others should represent just a single stem cell territory.

The majority of patches observed 5 weeks after pulse labeling consisted of labeled cells in the differentiating layers of the tubule (spermatocytes and/or spermatids), with no basal layer spermatogonia (type 1). Such patches contain no stem cells, as they are fated to exit when the labeled cells mature into sperm and are released. The other patches (types 2–4) did contain basal layer spermatogonia, and in addition, most contained labeled cells in the differentiating cell layers. In these patches, the labeled spermatogonia persisted while giving rise to differentiated progeny, indicating the presence of stem cells. We also noted that many of these "stem cell-derived" patches occupy only a part of the circumference of the seminiferous tubule, while a smaller part of them occupy the entire circumference. In Figure 4, those which occupy less than 50% of the circumference of the basal layer at their maximum were designated

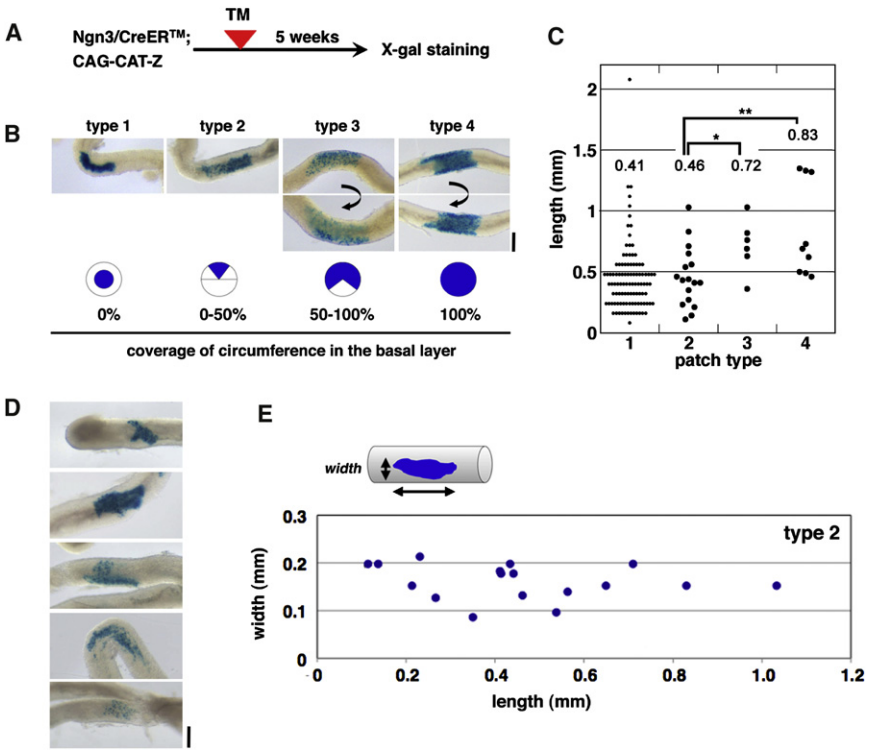

Figure 4. Young Patches 5 Weeks after Pulse Labeling

(A) Experimental schedule.

(B) Patches were classified into types 1–4, according to their maximal width around the seminiferous tubule. Type 1 patches contain no labeled basal layer cells, while patches of type 2–4 contain, respectively, <50%, 50%–100%, or 100% of the basal layer cells about the tubule circumference. Photos of typical patches for each type are also shown: the lower panels show the opposite side of the tubule. Bar, 200 μm (see Figure S3 for analysis of patch width over time).

(C) Length of patches according to type; for clarity, the type 1 data are shown rounded to the nearest 0.1 mm. The average lengths for each type is shown; (*) and (**) represent significant differences in the average, with p = 0.0203 and 0.0114, respectively, by t test.

(D) Appearance of the observed type 2 patches. Bar, 200 μm.

(E) Plot of length and width of type 2 patches.

type 2, those between 50%–100% type 3, and those that encircle the tubule (100%) were considered as type 4 (Figure 4B). Patches that occupy a larger fraction of the circumference were found to have a longer average patch length along the longitudinal axis of the tubules (Figure 4C). This suggests that individual stem cell-derived patches, on average, occupy a part of tubular circumference and that the type 2 patches can be used to estimate the size of a single stem cell-supported region. Indeed, the average length of the type 2 patches was 0.46 ± 0.06 mm (mean ± SEM), a value close to, but larger than, the independent estimations of l_0 mentioned above (<0.35 ± 0.08 mm and 0.37 ± 0.14 mm). Given that some type 2 patches would have already expanded along the length of the tubule, this is again consistent with the neutral drift theory and its quantitative predictions.

The measurement of the type 2 patches also suggests that individual stem cell-derived regions have a maximal width of 0.1 to 0.2 mm around the tubular circumference (Figures 4D and 4E), suggesting that between 4 and 6 stem cells surround the tubule circumference (0.609 ± 0.047 mm, average ± SD, n = 8). Interestingly, this number is commensurate with the number of blood vessels that surround a single tubule (determined by paraffin sectioning; 5.2 ± 0.8, mean ± SD, n = 107), which raises a possible relationship between the size of stem cell-derived patches and the arrangement of the vasculature. The preferential localization of the population of A_s, A_{pr}, and A_{al} to the vasculature that surrounds the seminiferous tubules, and their dispersion upon differentiation (Yoshida et al., 2007), also suggests that stem cell-supported regions might be anchored to the vasculature. In fact, the small patches found in testis sections at 5 weeks postlabeling were all found to be localized to the vasculature, and 3D reconstruction further reveals that the entire length of the small patches is aligned to the vasculature (Figures S3A and S3B). However, it remains to be shown whether the patches are indeed guided by the vasculature or whether the observed alignment results from independent constraints.

Stem Cell Replacement around the Seminiferous Tubule Circumference Follows the Same Neutral Drift Dynamics

A majority of 5-week-old stem cell-derived patches occupy less than half of the tubular circumference; however, this percentage decreased steadily throughout the experiment, while the fraction of clones surrounding the entire tubule circumference (i.e., Type 4) increased (Figures S3C–S3E). This indicates that stem cells also undergo replacement *around* the tubules as well as along the tubules. Does the expansion in clone width also follow the same neutral drift dynamics?

Our computer simulations, based on the simple lattice model in Figure 3B, provide a good quantitative fit to the fraction of Type 2, 3, and 4 patches over time, indicating that stem cells also undergo neutral drift around the tubules (Supplemental Experimental Procedures and Figures S3F and S3G). From this analysis, we can infer that the circumferential replacement time, τ_c, is close to that along the length, τ_l. A more realistic stem cell arrangement (Figure 3B, top), in which the number of neighboring stem cells is variable along the seminiferous tubule, would result in only small changes to estimates of τ_c without affecting any other conclusions of the analysis.

Stem Cell Migration over the Seminiferous Epithelium

We then moved on to experimentally challenge the prediction that stem cells are either replaced, or they multiply, at an average frequency of at least once in 2 weeks. This rate is surprisingly rapid, especially in comparison to more orthodox views of

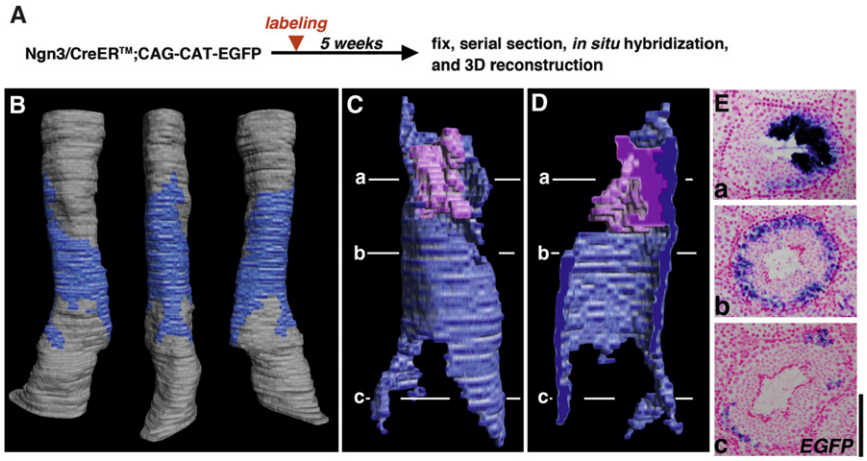

Figure 5. 3D Reconstruction of an Expanding Clone

(A) The experimental schedule.

(B) Reconstructed 3D image of a typical "type 4" patch observed 5 weeks after induction. The seminiferous tubule is represented (gray), with the area occupied by labeled spermatocytes and/or spermatids shown in blue. Views from three different orientations show that the patch covers the entire tubule circumference.

(C and D) 3D images of the distribution of labeled spermatids (purple; located in the innermost or 4th layer of the tubule), and pachytene spermatocytes (blue: in the 3rd layer) reconstituted from 107 serial sections. (C) and (D) represent the outer and sectioned view, respectively. Note that the labeled spermatids are restricted to only a small area of the clone, while younger pachytene spermatocytes are found along a much longer segment spanning the entire tubule circumference (see also Movie S1). This indicates the rapid expansion of the territory of the clone within one cycle of the seminiferous epithelium (i.e., 8.6 days). Labeled leptotene spermatocytes (in the 2nd layer) and spermatogonia (in the basal layer) were omitted from this reconstruction because of the difficulty in their precise localization owing to the lower expression of the reporter transgene in these cell types and the proximity to the intense signal in the pachytene spermatocytes (see E).

(E) The actual thin-section micrographs of the labeled cells visualized by in situ hybridization for EGFP (purple), with nuclei counterstained in red. (Ea), (Eb), and (Ec) correspond to the planes (Ca), (Cb), and (Cc) and (Da), (Db), and (Dc). Bar, 100 μm.

stem cells as long-lived entities that rarely turn over. Indeed, this result suggests that some stem cells could be replaced following just one seminiferous epithelial cycle, or 8.6 days. This possibility can be tested by a detailed morphological examination of the stem cell-derived patches: the history of the past territory of a single cell-derived clone is recapitulated by the area occupied by different layers of labeled differentiating germ cells, with a time resolution of 8.6 days (Figure 1D). We therefore analyzed the spatial distribution of labeled pachytene spermatocytes and spermatids in 5-week-old clones using 3D digital reconstructions from serial section micrographs (Figure 5 and Movie S1). In this patch, the region containing pachytene spermatocytes was significantly larger than the region containing spermatids (Figures 5C and 5D). This indicates that the single stem cell-derived territory expanded both along and around the tubules within 8.6 days. A similar discrepancy between layers was observed in all six serial-sectioned multilayered patches observed (data not shown). This supports the frequent and active turnover of stem cells in a time interval comparable to that predicted from the theory.

Second, we inferred that stem cell replacement requires frequent migration of spermatogonia over the seminiferous tubule. Therefore, we asked whether this is the case using in vivo live-imaging in mice transgenic for the Green Fluorescent Protein (GFP) controlled by the *ngn3* regulatory sequence (Figure 6 and Movie S2). As previously revealed (Yoshida et al., 2007), the population of A_s, A_{pr}, and A_{al} spermatogonia are localized to the vasculature-associated regions, and they delocalize and spread out over the seminiferous tubules upon undergoing differentiation into A_1 spermatogonia (Figure 6B). However, we also found that a small number of $Ngn3^+$ spermatogonia, including single A_s cells, actively migrated from one vascular-proximal region to another within a couple of days (a typical example is shown by green arrowheads in Figure 6B). Although the migratory activity of $GFR\alpha1^+$ (or $Nanos2^+$) spermatogonia, which are more closely related to the actual stem cells (Nakagawa et al., 2010; Sada et al., 2009), is yet to be elucidated, such rapid and ubiquitous migration of spermatogonia over the seminiferous tubule, including A_s cells, may provide the cellular basis for frequent stem cell replacement.

DISCUSSION

In this study, clone-fate data have revealed the stochastic dynamics of loss and renewal of equipotent stem cells derived from *ngn3* labeling. The loss of stem cells is not compatible with the traditional view of self-renewal proceeding through asymmetric division of a long-lived stem cell compartment, nor is there any evidence of predetermined heterogeneity in stem cell proliferative potential. Rather, the *entire* stem cell compartment actively turns over throughout life, with a surprisingly short lifetime (less than 2 weeks on average). This behavior can be directly inferred from the scaling analysis of the clone-fate data, which corresponds to a neutral drift in clone size; it is also consistent with the rapid basal layer expansion of clones and with in vivo live imaging showing that spermatogonial migration between adjacent vascular regions is common.

Interestingly, in comparison, extensive studies of germ line stem cells in the *Drosophila* ovary show that there too stem cells are turned over in homeostasis, with a half-life of 4 to 5 weeks (Jin et al., 2008; Xie and Spradling, 1998). The *Drosophila* ovary is anatomically separated into ~15 ovarioles, each of which contains two to three germ line stem cells localized to a discrete niche at the ovariolar distal pole (Xie and Spradling, 2000), and the germ line stem cells turn over within a single discrete niche. However, interniche replacement of stem cells has also been demonstrated in *Drosophila* ovarian follicle cells (Nystul and Spradling, 2007). This study raises the possibility that such stem cell turnover in *Drosophila* gonads occurs stochastically, as in mouse spermatogenesis.

In order to consider the processes involved in stem cell turnover, it is interesting to note that spermatogenesis and IFE

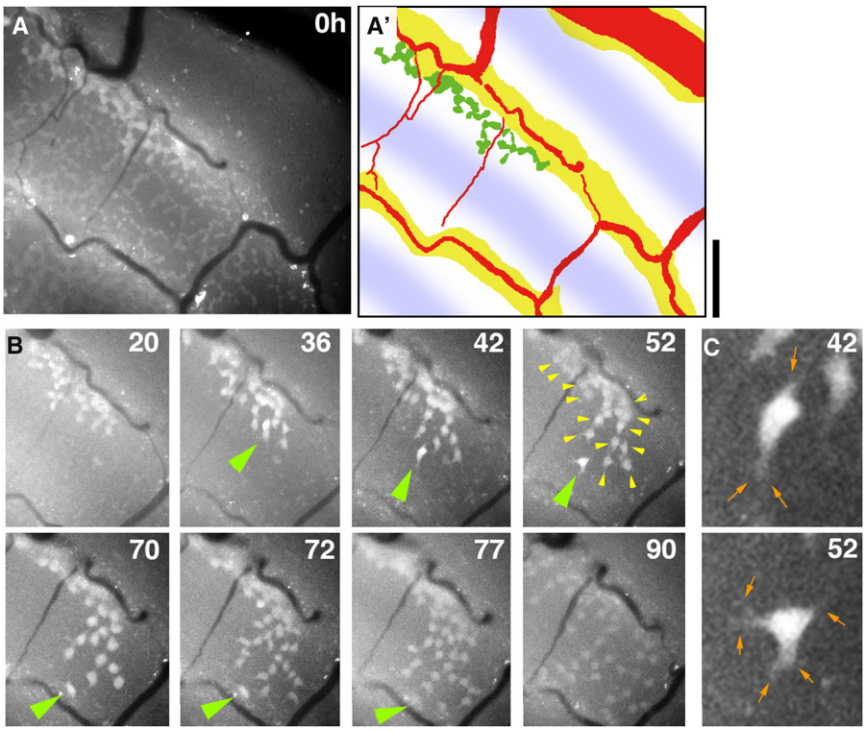

Figure 6. Migration of an A_s Spermatogonium between Niche Regions

Selected frames from live imaging of the testicular surface of an Ngn3/EGFP transgenic mouse (Movie S1).

(A) First frame of the film; (A′) indicates the position of undifferentiated spermatogonia (green), blood vessels (red) and interstitium (yellow). Continuity of the seminiferous tubules is shown by the wide blue stripes. Bar, 100 μm.

(B) Center of the field of view after the elapsed time indicated in hours. Green arrowheads indicate an A_s spermatogonium migrating out of the vasculature-proximal region, across the seminiferous tubules, and into another vasculature-related region. The remaining labeled undifferentiated spermatogonia form syncytial chains of $A_{aligned}$ (shown by yellow arrowheads in frames of 52 h), which depart from the vasculature-associated niche region, divide synchronously at 70-71 hr and spread over the seminiferous tubule. These behaviors indicate that during the movie the syncytia ($A_{aligned}$) transit into A_1 and then divide into A_2 spermatogonia (Yoshida et al., 2007).

(C) Magnified image of the migrating A_s spermatogonia at 42 and 52 hr, showing cytoplasmic extensions (orange arrows).

exhibit very similar, but distinct, neutral drift behaviors. In mouse IFE, clonal analysis shows that tissue is maintained by a single functionally equivalent cell population in which the balance between self-renewal and differentiation is achieved by a pattern of stochastic fate (Clayton et al., 2007; Doupé et al., 2010). In this case, the regulation of cell fate is cell-autonomous in that there is no correlation between the fates of neighboring cells. This leads to a linear growth of surviving clones with time. By contrast, in spermatogenesis, the labeled clones exhibit a square root growth, indicating that stem cell multiplication and loss are not cell-autonomous. Rather, multiplication is coupled with the loss of a neighboring stem cell.

How can such a local coupling of loss and multiplication of stem cells be achieved? One possibility is that, when a stem cell is lost by chance, one of the neighboring stem cells will sense this and divide symmetrically, giving rise to two stem cells. The new stem cell will then migrate along the tubule to replace the one that is lost. (Equally, stem cell multiplication could also trigger the loss of a neighboring stem cell). However, this mechanism presents several challenges. How could a stem cell sense the loss of a neighbor that is located at a distance spanning tens of cell diameters? What would guide the new stem cell to the correct location? What mechanism would ensure that just one out of several adjacent stem cells multiply in response to stem cell loss?

A second possibility, which is suggested by recent studies of A_s, A_{pr}, and A_{al} self-renewal, is that spermatogonial subpopulations with different self-renewing probabilities *collectively* form the stem cell compartment. While GFRα1$^+$ (and probably also Nanos2$^+$) A_s cells appear to have the highest probability of generating long-lived clones, the Ngn3$^+$/GFRα1$^-$ spermatogonia (mostly syncytial cysts of A_p and A_{al}), which normally proceed to differentiate, can also give rise to persisting clones including GFRα1$^+$ A_s cells through cyst fragmentation and a change in gene expression (Nakagawa et al., 2010, schematically shown in Figure 1E). Intriguingly, the probability of such "reversion" rises when stem cells are lost (Nakagawa et al., 2010). These observations suggest a hypothesis in which steady-state spermatogenesis is supported by an extended population of spermatogonia that are prone to differentiation but migrate laterally along the tubules before undergoing fate commitment. This allows the cells to switch to self-renewal by "reverting" to a GFRα1$^+$ state after migrating into an adjacent region lacking stem cells. As a result, stem cell multiplication will be coupled to the loss of a neighboring stem cell, precisely fitting the observed neutral drift dynamics. Importantly, the questions raised above for the first possibility do not arise at all in this case. Moreover, based on this second scenario, stem cells should be replaced by their own progeny more frequently than by that of the neighboring stem cells. This suggests that stem cells are replaced even more frequently than estimated in this study, in which only stem cell replacement between different clones can be captured. Furthermore, this scenario suggests that the stem cell population might not be clearly defined by their expression of *GFRα1* or *nanos2*; instead, spermatogenesis might be supported by a pool of spermatogonia with the same potential for long-term self-renewal, in which some are more likely to self-renew, while their progeny are primed for differentiation but are not committed to this fate.

It is tempting to ask whether the patterns of neutral drift and frequent stem cell replacement are indicative of a deeper role for stochasticity in the maintenance of cycling tissues.

Intriguingly, neutral drift implies a pattern of stem cell regulation in which the processes of self-renewal and differentiation are naturally balanced. As adjacent clones compete to maintain a constant number of stem cells, the rates of stem cell activity become "self-tuned": an increase in stem cell differentiation, or loss, leads to a corresponding increase in renewal, and vice versa. Such self-tuning lies at the very foundation of neutral drift of the labeled clones, leading to their stochastic incremental expansion, contraction, and subsequent extinction. It is therefore likely that stochastic fate may indeed be a universal feature of all spatially extended, rapidly cycling adult tissues.

EXPERIMENTAL PROCEDURES

Animals

Ngn3/CreER™ (Yoshida et al., 2006), CAG-CAT-LacZ (Araki et al., 1995), CAG-CAT-EGFP (Kawamoto et al., 2000), and Ngn3/EGFP (Yoshida et al., 2004) transgenic mice were maintained and crossed to obtain appropriate double transgenic mice under the C57BL/6 background (purchased from Japan Clea and Japan SLC). All the experiments and animal protocols were approved by the Institutional Animal Care and Use Committee of National Institutes of Natural Sciences and Animal Research Committee, Kyoto University.

Pulse Labeling and Analysis of Induced Patches

Ngn3/CreER™;CAG-CAT-Z double transgenic mice were injected with tamoxifen at the age of 2 months. After appropriate periods of time, patches of the pulse-labeled cells were visualized by X-gal staining as described previously (Nakagawa et al., 2007). The LacZ-positive patches were photographed and their size measured using a DMRBE microscope (Leica) equipped with an Axiocam CCD camera and Axiovision software (Zeiss Vision). The diameter of the tubules was measured in the same manner.

3D Reconstruction of Pulse-Labeled Patches

Ngn3/CreER™;CAG-CAT-Z double-transgenic adult mice were injected with 4OH-tamoxifen (2 mg/individual dissolved in sesame oil, as previously described for tamoxifen [Nakagawa et al., 2007]). Five weeks later, testes were removed and processed for in situ hybridization for EGFP mRNA (Clonetech) on paraffin sections (7 μm thick), as described (Yoshida et al., 2004). After visualizing the EGFP-positive labeled cells in purple, specimens were counterstained with nuclear fast red and photographed. Subsequent 3D reconstruction was performed using Photoshop (Adobe) and DeltaViewer (http://delta.math.sci.osaka-u.ac.jp/DeltaViewer/) software as described (Yoshida et al., 2007).

Live Imaging of Ngn3$^+$ Spermatogonia in the Testis

Live imaging of the Ngn3/EGFP mouse testis was performed as described (Yoshida et al., 2007).

Scaling Analysis and Modeling

Isolated patches were scored as single clones and size distributions were constructed as described in supplementary methods. Analysis of size distributions and fits to power law growth were conducted using MATLAB (R2008b) and XMGRACE (Grace-5.1.22). Theoretical analysis of the 1D and 2D neutral drift models, and the models ruled out by the data, are described in Supplemental Experimental Procedures.

SUPPLEMENTAL INFORMATION

Supplemental Information includes three figures, Supplemental Experimental Procedures, and two movies and can be found with this article online at doi:10.1016/j.stem.2010.05.017.

ACKNOWLEDGMENTS

We are grateful to A. Philpott and T. Ogawa for their insightful comments and discussions. We thank Y. Nabeshima for his continuous support and encouragement, R Sugimoto for discussions and technical instruction, and M. Sukeno and T. Obata for their technical assistance. We also thank T. Sasaoka and the staff of the Division of Model Animal Research, NIBB Bio-Resource Center, and Institute of Laboratory Animals, Graduate School of Medicine, Kyoto University, for support on animal experiments. The experimental work was partly supported by Grant-in-Aid for Scientific Research (KAKENHI) on Innovative Areas, 'Regulatory Mechanism of Gamete Stem Cells' from MEXT, Japan to S.Y. (no. 20116004). A.M.K. is supported by an EPSRC LSI fellowship ref. EP/F043325/1.

Received: October 19, 2009
Revised: March 25, 2010
Accepted: May 12, 2010
Published: August 5, 2010

REFERENCES

Araki, K., Araki, M., Miyazaki, J., and Vassalli, P. (1995). Site-specific recombination of a transgene in fertilized eggs by transient expression of Cre recombinase. Proc. Natl. Acad. Sci. USA *92*, 160–164.

Bachelier, L. (1900). Théorie de la spéculation; Théorie mathématique du jeu, Reprod. en fac-sim. edn (Paris: Ed. J. Gabay).

Barroca, V., Lassalle, B., Coureuil, M., Louis, J.P., Le Page, F., Testart, J., Allemand, I., Riou, L., and Fouchet, P. (2009). Mouse differentiating spermatogonia can generate germinal stem cells in vivo. Nat. Cell Biol. *11*, 190–196.

Brown, J.H., and West, G.B.; Santa Fe Institute. (2000). Scaling in biology (New York: Oxford University Press).

Clayton, E., Doupé, D.P., Klein, A.M., Winton, D.J., Simons, B.D., and Jones, P.H. (2007). A single type of progenitor cell maintains normal epidermis. Nature *446*, 185–189.

de Rooij, D.G., and Russell, L.D. (2000). All you wanted to know about spermatogonia but were afraid to ask. J. Androl. *21*, 776–798.

Doupé, D.P., Klein, A.M., Simons, B.D., and Jones, P.H. (2010). The ordered architecture of murine ear epidermis is maintained by progenitor cells with random fate. Dev. Cell *18*, 317–323.

Jin, Z., Kirilly, D., Weng, C., Kawase, E., Song, X., Smith, S., Schwartz, J., and Xie, T. (2008). Differentiation-defective stem cells outcompete normal stem cells for niche occupancy in the Drosophila ovary. Cell Stem Cell *2*, 39–49.

Kawamoto, S., Niwa, H., Tashiro, F., Sano, S., Kondoh, G., Takeda, J., Tabayashi, K., and Miyazaki, J. (2000). A novel reporter mouse strain that expresses enhanced green fluorescent protein upon Cre-mediated recombination. FEBS Lett. *470*, 263–268.

Kimura, M. (1983). The neutral theory of molecular evolution (New York: Cambridge University Press).

Nakagawa, T., Nabeshima, Y., and Yoshida, S. (2007). Functional identification of the actual and potential stem cell compartments in mouse spermatogenesis. Dev. Cell *12*, 195–206.

Nakagawa, T., Sharma, M., Nabeshima, Y., Braun, R.E., and Yoshida, S. (2010). Functional hierarchy and reversibility within the murine spermatogenic stem cell compartment. Science *328*, 62–67.

Nystul, T., and Spradling, A. (2007). An epithelial niche in the Drosophila ovary undergoes long-range stem cell replacement. Cell Stem Cell *1*, 277–285.

Russell, L., Ettlin, R., Sinha Hikim, A., and Clegg, E. (1990). Histological and histopathological evaluation of the testis (Clearwater, FL: Cache River Press).

Sada, A., Suzuki, A., Suzuki, H., and Saga, Y. (2009). The RNA-binding protein NANOS2 is required to maintain murine spermatogonial stem cells. Science *325*, 1394–1398.

Simon, A., and Frisén, J. (2007). From stem cell to progenitor and back again. Cell *128*, 825–826.

Spence, A.J. (2009). Scaling in biology. Curr. Biol. *19*, R57–R61.

Suzuki, H., Sada, A., Yoshida, S., and Saga, Y. (2009). The heterogeneity of spermatogonia is revealed by their topology and expression of marker proteins including the germ cell-specific proteins Nanos2 and Nanos3. Dev. Biol. *336*, 222–231.

Xie, T., and Spradling, A.C. (1998). decapentaplegic is essential for the maintenance and division of germline stem cells in the Drosophila ovary. Cell *94*, 251–260.

Xie, T., and Spradling, A.C. (2000). A niche maintaining germ line stem cells in the Drosophila ovary. Science *290*, 328–330.

Yoshida, S., Takakura, A., Ohbo, K., Abe, K., Wakabayashi, J., Yamamoto, M., Suda, T., and Nabeshima, Y. (2004). Neurogenin3 delineates the earliest stages of spermatogenesis in the mouse testis. Dev. Biol. *269*, 447–458.

Yoshida, S., Sukeno, M., Nakagawa, T., Ohbo, K., Nagamatsu, G., Suda, T., and Nabeshima, Y. (2006). The first round of mouse spermatogenesis is a distinctive program that lacks the self-renewing spermatogonia stage. Development *133*, 1495–1505.

Yoshida, S., Sukeno, M., and Nabeshima, Y. (2007). A vasculature-associated niche for undifferentiated spermatogonia in the mouse testis. Science *317*, 1722–1726.